ECAS 2020

sciforum

*Conference Proceedings Paper*

# Optical properties and direct radiative effects of aerosol species at global scale based on the synergistic use of MERRA-2 optical properties and the FORTH radiative transfer model

**Marios-Bruno Korras-Carraca [1,2], Antonis Gkikas [3], Arlindo M. Da Silva [4], Christos Matsoukas [2,*], Nikolaos Hatzianastassiou [1] and Ilias Vardavas [5]**

[1] Laboratory of Meteorology, Department of Physics, University of Ioannina, Ioannina, Greece; e-mail@e-mail.com
[2] Department of Environment, University of the Aegean, Mytilene, Greece;
[3] Institute for Astronomy, Astrophysics, Space Applications and Remote Sensing (IAASARS), National Observatory of Athens, Athens, Greece;
[4] NASA/GSFC, Greenbelt, MD 20771, USA;
[5] Department of Physics, University of Crete, 71110 Heraklion, Crete, Greece;
* Correspondence: nhatzian@uoi.gr (N-H); koras@env.aegean.gr (MB -KC)

Received: date; Accepted: date; Published: date

**Abstract:** The overarching goal of the current study is to quantify the aerosol induced clear-sky direct radiative effects (DREs) within the Earth-Atmosphere system at global scale and for the 40-year period 1979-2019. To this aim, the MERRA-2 aerosol radiative properties, along with meteorological fields and surface albedo, are utilized as inputs to the FORTH radiative transfer model (RTM). Our preliminary results, representative for the year 2015, reveal strong surface radiative cooling (down to -45 $Wm^{-2}$) over areas where high aerosol loadings and absorbing particles (i.e., dust and biomass burning) dominate. This reduction of the incoming solar radiation, in the aforementionned regions, is largely attributed to its absorption by the overlying suspended particles resulting in an atmospheric warming reaching up to 40 $Wm^{-2}$. At the top-of-atmosphere (TOA) negative DREs (planetary cooling) are computed worldwide (down to -20 $Wm^{-2}$) with few exceptions over bright surfaces (warming up to 5 $Wm^{-2}$). Finally, the strong variations between the obtained DREs of different aerosol species (dust, sea-salt, sulphate, organic/black carbon) as well as between hemispheres and surface types (i.e., land vs ocean) are also discussed.

**Keywords:** aerosols; aerosol direct radiative effects; global aerosol reanalysis

## 1. Introduction

Aerosols, among other atmospheric constituents, through their interaction with radiation, exert a perturbation of the Earth-Atmosphere system energy budget, thus playing a key role in the current and future climate. Originating from natural and anthropogenic sources worldwide, the microphysical and optical properties of the suspended particles, which determine the aerosol-radiation interactions, reveal a remarkable variability both in space and time. Moreover, the vertical structure of aerosol layers as well as the underlying surface properties impose a further complexity in the assessment of the relevant radiative effects under clear-sky conditions. In order to quantify the aerosol radiative effects, at global and regional scales, it is required an accurate speciation of tropospheric and stratospheric aerosol types as well as an optimum characterization of their key radiative properties, namely the aerosol optical depth (AOD), single scattering albedo (SSA) and asymmetry parameter (g). Such challenging tasks can be fulfilled either by observations or modelling techniques, which are both characterized by specific advantages and drawbacks. A comprehensive analysis in aerosol-radiation studies requires the estimation of radiative affects per each aerosol type and their contribution to the total perturbation at long-term (i.e. decadal) scales aiming at reducing the current uncertainty levels reported by the Intergovernmental Panel of Climate Change (IPCC) [1].

In this study, we use the full dataset of MERRA-2 reanalysis aerosol optical properties [2,3], spanning over four decades (1979-2019), along with a radiation transfer model (RTM) in order to investigate the spatio-temporal distribution of the clear-sky direct radiative effects (DREs) per aerosol type as well as for the total aerosol load. As a demonstration of our analysis, we present here preliminary results, referring to the year 2015, for the perturbed radiation fields at the top-of-the-atmosphere (TOA), within the atmosphere and at the surface.

## 2. Methods

The aerosol DREs are computed using the deterministic spectral radiation transfer model FORTH [4], developed from a radiative-convective model [5]. The model computations are performed on a monthly 0.5° × 0.625° horizontal resolution (the original MERRA-2 resolution). The monochromatic radiative flux transfer equations are solved in 118 wavelengths between 0.20 and 1 μm and 10 spectral intervals between 1 and 10 μm, assuming an absorbing/ multiple-scattering atmosphere and using the Delta-Eddington method.

In order to calculate the aerosol DRE, the model requires their vertically and spectrally resolved optical properties (i.e. AOD, SSA, and g). However, MERRA-2 does not provide directly such data. Therefore, we computed them based on 3-hourly vertically resolved instantaneous aerosol mixing ratios and relative humidity data (both included in the MERRA-2 reanalysis and provided in 72 vertical layers) and look-up tables that provide the scattering and absorption efficiencies per aerosol type, aerosol size bin, relative humidity, and 25 wavelength. Apart from aerosols, all

remaining RTM required input data (surface albedo, specific humidity and ozone concentration) are also taken from MERRA-2.

The aerosol DREs are computed at the Earth's surface, within the atmosphere and at the Top of the Atmosphere (TOA) as

$$DRE_x = F_{aer} - F_{no\text{-}aer\text{-}x}, \quad (1)$$

where x corresponds to the aerosol type (sulfate, sea-salt, dust, organic carbon, black carbon and total) $F_{aer}$ are the net downward (downward minus upward) radiative fluxes obtained running the RTM with all aerosol types and $F_{no\text{-}aer\text{-}x}$ the corresponding fluxes computed with the RTM without considering a particular aerosol type x (in the case of x=total, $F_{no\text{-}aer\text{-}x}$ corresponds to an atmosphere without any aerosols).

## 3. Results and discussion

### *3.1. Aerosol optical properties for the year 2015*

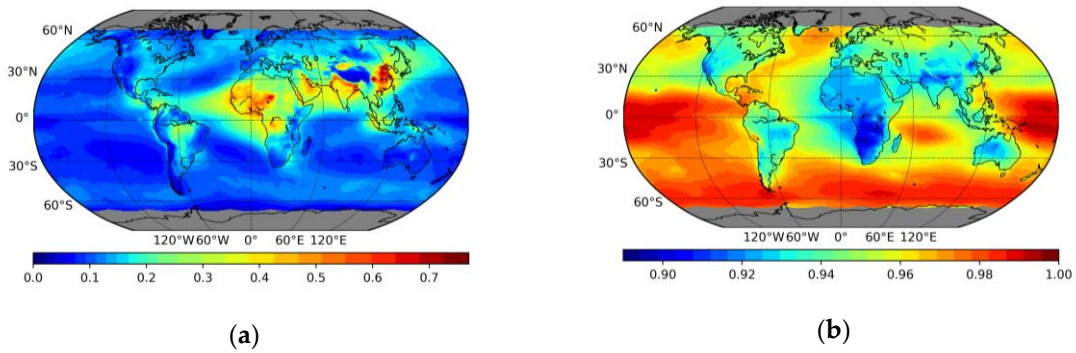


**Figure 1.** Mean annual (2015) global distribution of MERRA-2 optical properties for the total aerosol load at 550 nm: (**a**) Aerosol optical depth; (**b**) Single scattering albedo.

We begin this section with a brief presentation of the main patterns of the geographic variation of the MERRA-2 AOD and SSA. As shown in Figure 1a, a significant spatial variability of the AOD is evident. The highest aerosol load (up to 0.77, on a mean annual level) is observed at east China. In this region, according to our MERRA-2 (results not shown here) the aerosol load is dominated by sulfate particles, but also by significant loads of carbonaceous (organic and black carbon) particles. Equally high aerosol load (AOD up to 0.73) is observed in North Africa, especially above the dust dominated southern and south-western parts of the Sahara Desert and the western sub-Sahel. Over the latest region, besides the advected desert dust, there is also a strong presence of carbonaceous particles (organic and black carbon) originating from biomass burning taking place during winter (dry season). High aerosol load is observed over most arid and semi-arid regions of the planet, with AOD reaching 0.50 over the Arabian Peninsula and 0.45 over the Taklamakan desert. Over the Indian subcontinent, the presence of significant aerosol sources (both natural, such as the Thar Desert, and anthropogenic) results in AOD values

that are generally larger than 0.30 and reach 0.53 over the Indo-Gangetic Plain. High aerosol loads are also evident over regions with frequent seasonal biomass burning, and therefore strong presence of carbonaceous particles. Thus, AOD values reach up 0.46 over the central-southern Africa, 0.34 over the Maritime Southeast Asia, 0.25 over South America and 0.17 over North-Western America. On the other hand, aerosol load is low (AOD less than 0.1) above most oceanic regions. However, in the case of long-range transport of continental particles above oceanic regions, the aerosol load may be very high. Such a characteristic case is the Saharan dust and biomass burning outflows to the tropical and subtropical North Atlantic Ocean and the Gulf of Guinea, resulting in AOD as high as 0.40. Other oceanic regions with relatively high aerosol load are the tropical South Atlantic, where mainly carbonaceous particles are transported from the African continent, and the North Indian Ocean (transportation of both natural and anthropogenic particles from the Indian Subcontinent and the Arabian Peninsula).

The aerosol SSA values (Figure 1b) range between 0.89 and 1.0. The lowest values (deep blue colors) are observed over regions where the aerosol load is dominated by biomass burning aerosols including the strong absorptive black carbon particles. The most characteristic region with low SSA values (generally lower than 0.92) is the Central and Southern Africa. Relatively low SSA is also observed above eastern and southern Asia, the Sahara Desert, western United States, western Europe and the tropical Atlantic Ocean. On the other hand, over most remote oceanic regions, the SSA is high due to the dominance of non-absorbing sea-salt particles.

*3.2 Aerosol radiative effects for the year 2015*

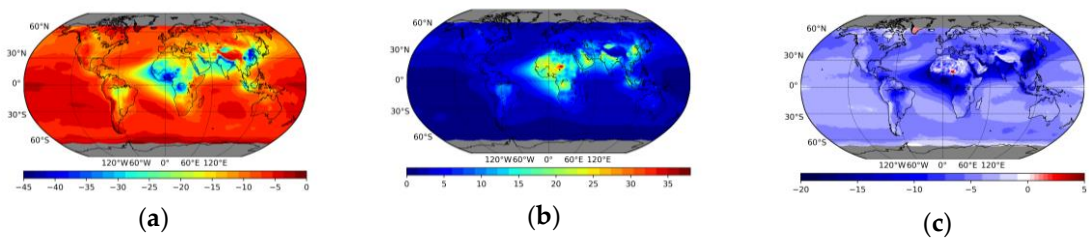


**Figure 3.** Mean annual (2015) global distribution of aerosol direct radiative effect ($Wm^{-2}$): (**a**) at the Earth's surface; (**b**) within the atmosphere; (**c**) at the Top Of Atmosphere (TOA).

The mean annual geographical distribution of the aerosol effects on the net shortwave flux at the Earth's surface (hereafter $DRE_{surfnet}$), within the atmosphere ($DRE_{atm}$) and at TOA ($DRE_{TOA}$) for the year 2015 is presented in Figure 3.

At the Earth's surface (Figure 3a), aerosol cause a cooling effect (negative $DRE_{surfnet}$). This cooling is associated with the reduction of the downwelling solar radiation due to scattering and absorption by aerosol particles and is more

pronounced over regions with high aerosol load. More specifically, the strongest cooling effect (up to -42 $Wm^{-2}$) is observed over east China, which is characterized by high loads of strongly scattering sulfate particles. A strong cooling effect is also evident over North Africa (strong presence of desert dust and carbonaceous particles), with $DRE_{surfnet}$ ranging between -15 and -35 $Wm^{-2}$ over most of the Sahara Desert and reaching -40 $Wm^{-2}$ in the Sub-Sahel (Niger delta region). A pronounced cooling effect is observed over Central Africa ($DRE_{surfnet}$ -20 to -38 $Wm^{-2}$), the Indo-Gangetic Plain (cooling up to 40 $Wm^{-2}$ locally), the Arabian Peninsula as well as above neighboring oceanic regions where aerosols are transported from the former source areas.

The aerosol effect within the atmosphere (hereafter $DRE_{atm}$) is presented in Figure 3b. It is evident that aerosols cause a heating of the atmosphere (by increasing the atmospheric absorption). This heating effect is stronger in regions with high aerosol loads and absorbing particles, characterized by relatively low SSA. Although $DRE_{atm}$ has an opposite sign to that of $DRE_{surfnet}$, their geographic distributions are similar. The atmospheric heating is especially pronounced above North Africa ($DRE_{atm}$ up to 38 $Wm^{-2}$ over the Southern Saharan Desert). A relatively strong aerosol heating is also observed above the Arabian Peninsula (up to 24 $Wm^{-2}$). Over the biomass burning dominated Central Africa, and the highly populated Southern and Eastern Asia, aerosols cause an atmospheric heating equal to 20-24 $Wm^{-2}$ locally.

The geographical distribution of the aerosol effect at the top-of-the-atmosphere (hereafter $DRE_{TOA}$) is shown in Figure 3c. The values of $DRE_{TOA}$ range between -21 to 5 $Wm^{-2}$. Negative values indicate decreasing net incoming solar radiation (i.e. planetary cooling due to increased backscattered solar radiation to space), while positive indicate a planetary warming. It is evident that aerosols cause a cooling effect above most parts of globe. This planetary cooling is much more pronounced ($DRE_{TOA}$ ranging between -10 to -20 $Wm^{-2}$) over the Sahel and Sub-Sahel, Central Africa, the Indian Subcontinent and Eastern China, namely over regions characterized by high aerosol load of both natural and anthropogenic origin. A strong planetary cooling is also observed above oceanic regions where continental aerosols are advected (such as the tropical Atlantic Ocean and the Northern Indian Ocean). Note that over the Arabian Peninsula and the Sahara Desert $DRE_{TOA}$ is relatively low, despite the presence of high loads of desert dust. In some parts of the Sahara Desert there is even a planetary warming effect (up to 4-5 $Wm^{-2}$, locally). These arid regions are characterized by strong surface albedo (greater than 0.25) resulting in multiple scattering between relatively absorbing desert dust particles and the ground [6,7]. Therefore, there is a near-cancellation of the surface cooling by an equally large atmospheric warming over most parts of these regions. The aerosol planetary heating effect is observed over the parts of Sahara with the highest surface albedo, highlighting the importance of this parameter for the determination of the sign of $DRE_{TOA}$. The small planetary heating observed over the ice covered southern Greenland can also be explained by the very high surface albedo therein.

**Table 1.** Annual averaged total aerosol DREs (in $Wm^{-2}$) for 2015 over: the globe, the North and South Hemispheres, global land and global ocean areas. The corresponding averages for AOD and SSA at 550 nm are shown in the last columns.

| | $DRE_{TOA}$ | $DRE_{atm}$ | $DRE_{surfnet}$ | AOD | SSA |
|---|---|---|---|---|---|
| Global | -4.79 | 3.94 | -8.73 | 0.137 | 0.957 |
| Land | -5.33 | 6.66 | -11.98 | 0.172 | 0.938 |
| Ocean | -4.55 | 2.72 | -7.27 | 0.121 | 0.965 |
| N. Hemisphere | -5.64 | 5.41 | -11.05 | 0.171 | 0.950 |
| S. Hemisphere | -3.96 | 2.50 | -6.46 | 0.104 | 0.963 |

The globally and hemispherically averaged values of the aerosol DREs, as well as the DREs averaged over global land and ocean areas are presented in Table 1. Under clear-sky conditions, aerosols cause a cooling effect of -8.73 $Wm^{-2}$ at the Earth's surface and a warming of the atmosphere equal to 3.94 $Wm^{-2}$. The surface cooling is larger in magnitude than the atmospheric warming effect, therefore aerosol particles cause a planetary cooling effect at TOA of -4.79 $Wm^{-2}$. The aerosol DREs exhibit differences in their magnitude between land and oceans as well as between the two hemispheres. The aerosol effects are larger over land than over ocean and over the North Hemisphere compared to the South. These differences are more pronounced for the $DRE_{atm}$ and they are related to the presence of stronger and more absorbing aerosols over the North Hemisphere and global land areas.

**Table 2.** Annual averaged sulfate aerosol DREs (in $Wm^{-2}$) for 2015 over: the globe, the North and South Hemispheres, global land and ocean areas. The same averages for scattering and absorption AOD at 550 nm are shown in the last two columns.

| | $DRE_{TOA}$ | $DRE_{atm}$ | $DRE_{surfnet}$ | $AOD_{sct}$ | $AOD_{abs}$ |
|---|---|---|---|---|---|
| Global | -0.96 | 0.46 | -1.42 | 0.036 | 0.000 |
| Land | -1.46 | 0.43 | -1.90 | 0.054 | 0.000 |
| Ocean | -0.73 | 0.48 | -1.21 | 0.028 | 0.000 |
| N. Hemisphere | -1.41 | 0.45 | -1.86 | 0.051 | 0.000 |
| S. Hemisphere | -0.51 | 0.48 | -0.99 | 0.021 | 0.000 |

**Table 3.** Annual averaged desert dust aerosol DREs (in $Wm^{-2}$) for 2015 over: the globe, the North and South Hemispheres, global land and ocean areas. The same averages for scattering and absorption AOD at 550 nm are shown in the last two columns.

| | $DRE_{TOA}$ | $DRE_{atm}$ | $DRE_{surfnet}$ | $AOD_{sct}$ | $AOD_{abs}$ |
|---|---|---|---|---|---|
| Global | -0.61 | 1.72 | -2.33 | 0.028 | 0.002 |
| Land | -1.24 | 3.13 | -4.36 | 0.056 | 0.004 |
| Ocean | -0.33 | 1.09 | -1.41 | 0.015 | 0.001 |
| N. Hemisphere | -1.27 | 2.69 | -3.96 | 0.049 | 0.004 |

| | | | | | |
|---|---|---|---|---|---|
| S. Hemisphere | 0.04 | 0.77 | -0.73 | 0.007 | <0.001 |

**Table 4.** Annual averaged sea salt aerosol DREs (in $Wm^{-2}$) for 2015 over: the globe, the North and South Hemispheres, global land and ocean areas. The same averages for scattering and absorption AOD at 550 nm are shown in the last two columns.

| | $DRE_{TOA}$ | $DRE_{atm}$ | $DRE_{surfnet}$ | $AOD_{sct}$ | $AOD_{abs}$ |
|---|---|---|---|---|---|
| Global | -1.23 | 0.59 | -1.82 | 0.042 | 0.000 |
| Land | -0.14 | 0.47 | -0.61 | 0.014 | 0.000 |
| Ocean | -1.73 | 0.64 | -2.37 | 0.055 | 0.000 |
| N. Hemisphere | -0.92 | 0.55 | -1.47 | 0.035 | 0.000 |
| S. Hemisphere | -1.55 | 0.63 | -2.17 | 0.049 | 0.000 |

**Table 5.** Annual averaged organic carbon aerosol DREs (in $Wm^{-2}$) for 2015 over: the globe, the North and South Hemispheres, global land and ocean areas. The same averages for scattering and absorption AOD at 550 nm are shown in the last two columns.

| | $DRE_{TOA}$ | $DRE_{atm}$ | $DRE_{surfnet}$ | $AOD_{sct}$ | $AOD_{abs}$ |
|---|---|---|---|---|---|
| Global | -0.72 | 0.73 | -1.45 | 0.025 | <0.001 |
| Land | -1.36 | 0.87 | -2.22 | 0.039 | 0.001 |
| Ocean | -0.44 | 0.66 | -1.10 | 0.018 | <0.001 |
| N. Hemisphere | -0.85 | 0.73 | -1.58 | 0.028 | <0.001 |
| S. Hemisphere | -0.60 | 0.72 | -1.33 | 0.022 | <0.001 |

**Table 6.** Annual averaged black carbon aerosol DREs (in $Wm^{-2}$) for 2015 over: the globe, the North and South Hemispheres, global land and ocean areas. The same averages for scattering and absorption AOD at 550 nm are shown in the last two columns.

| | $DRE_{TOA}$ | $DRE_{atm}$ | $DRE_{surfnet}$ | $AOD_{sct}$ | $AOD_{abs}$ |
|---|---|---|---|---|---|
| Global | 0.69 | 2.33 | -1.64 | 0.002 | 0.004 |
| Land | 0.97 | 3.48 | -2.51 | 0.002 | 0.007 |
| Ocean | 0.57 | 1.81 | -1.24 | 0.001 | 0.003 |
| N. Hemisphere | 0.83 | 2.78 | -1.94 | 0.002 | 0.005 |
| S. Hemisphere | 0.56 | 1.90 | -1.34 | 0.001 | 0.004 |

In Tables 2-6 we provide the averaged DREs of each aerosol particle type (i.e. sulfate,dust,sea salt, organic carbon and black carbon) separately, in order to provide some insight about their contribution to the total aerosol effect. From these results, large differences between the DREs of different particle type are evident. More specifically, the strongest cooling effect on the Earth' surface is caused by desert dust (-2.33 $Wm^{-2}$) followed by sea-salt, black, organic carbon and sulfate particles (-1.42 $Wm^{-2}$). The atmospheric heating is proportional to the particle

absorptivity. Therefore, strongest heating (2.33 $Wm^{-2}$) is caused by black carbon particles, followed by dust (1.72 $Wm^{-2}$), while the heating effect of the almost purely scattering sea-salt and sulfate is small. The non-zero $DRE_{atm}$ of scattering sea-salt and sulfate aerosols is possibly related to the increase of the surface back-scattered radiation they cause, and therefore the increase of the available radiative energy, which results in an increased absorption by other (absorbing) aerosol types and atmospheric gases above sea-salt and sulfate aerosol layers. At TOA, all particles except black carbon cause a cooling effect. The strongest TOA cooling is observed for sea-salt and sulfate (-1.23 $Wm^{-2}$ and -0.96 $Wm^{-2}$, respectively). The $DRE_{TOA}$ caused by organic carbon and dust particles is also negative (however smaller than the effect of sea-salt and sulfate). On the other hand, black carbon particles, despite their relatively small optical depth, cause a substantial TOA heating equal to 0.69 $Wm^{-2}$, due to their strong absorptivity. This depicts the important climatic role of black carbon particles.

## 4. Conclusions

In this study, MERRA-2 aerosol optical properties and the FORTH deterministic spectral radiative transfer model we used in order to compute the aerosol direct radiative effect (DRE) under clear-sky conditions at the Earth's surface, within the atmosphere, and at the Top Of the Atmosphere (TOA), for 2015 on a global scale. It is found that aerosols cause a cooling of the Earth's surface (-8.73 $Wm^{-2}$) and a warming of the atmosphere (3.94 $Wm^{-2}$). These effects were found to be stronger in regions with high aerosol loads, especially consisted of absorbing particles. The aerosol induced reduction of solar radiation at the Earth's surface contributes to global dimming, and is very important for climate, because it can reduce the evaporation rates, leading eventually to a slowdown of the water cycle [8,9]. The atmospheric warming caused by aerosols, in combination with the surface cooling, can result in a stabilization of the atmosphere, and therefore to a suppress of cloud formation [10,11], enhancing desertification processes [7]. Overall, aerosols result in a planetary TOA cooling effect above most of the globe, with the exception of a few regions with high surface albedo, such as parts of the Saharan Desert and Greenland, where aerosols cause a planetary warming. In general, the aerosol DREs are larger over the North than South Hemisphere and over land than ocean areas. Profound differences are found between the obtained DREs for different aerosol types. The strongest TOA cooling effect is found for sea-salt and sulfate aerosols (-1.23 and -0.96 $Wm^{-2}$, respectively) while black carbon aerosols cause a planetary warming (-0.69 $Wm^{-2}$). Future work will focus on the determination of long-term DREs as well as the DREs' inter-annual and decadal scale variations in relation with global dimming and brightening and contribution to climate change.

**Author Contributions:** Conceptualization, N.H. and A.G.; methodology, N.H., C.M. and A.G.; software, N.H., C.M. and I.V.; formal analysis, M.K.C.. and A.G.; investigation, N.H., C.M., A.G. and M.K.C; resources, I..V., N.H., C.M. and A.S.; data curation, M.K..C. and A.G.; writing—original draft preparation, M.K..V. and A.G.; writing—review and editing, N.H.; visualization, M.K.C.; supervision, N.H. and C.M.; project administration, N.H..; funding acquisition, N.H. All authors have read and agreed to the published version of the manuscript.", please turn to the CRediT taxonomy for the term explanation.

**Funding:** This research was funded by the programme "Support for researchers with an emphasis on young researchers - cycle B'" of the General Secretariat for Research and Technology-Hellas., grant number 1052"

**Acknowledgments:** In this section you can acknowledge any support given which is not covered by the author contribution or funding sections. This may include administrative and technical support, or donations in kind (e.g., materials used for experiments).

**Conflicts of Interest:** The authors declare no conflict of interest. The funders had no role in the design of the study; in the collection, analyses, or interpretation of data; in the writing of the manuscript, or in the decision to publish the results.

## References

1. Boucher, O.; Randall, D.; Artaxo, P.; Bretherton, C.; Feingold, G.; Forster, P.; Kerminen, V.-M.; Kondo, Y.; Liao, H., Lohmann, U.; Rasch, P.; Satheesh, S. K.; Sherwood, S.; Stevens, B.,; Zhang, X. Y. Clouds and Aerosols, in: Climate Change 2013: The Physical Science Basis, Contribution of Working Group I to the Fifth Assessment Report of the Intergovernmental Panel on Climate Change; Stocker, T. F., Qin, D., Plattner, G.-K., Tignor, M., Allen, S. K., Boschung, J., Nauels, A., Xia, Y., Bex, V. and Midgley, P. M., Eds. Cambridge University Press: Cambridge, UK and New York, NY, USA, 2013 pp. 571–658
2. Gelaro, R.; McCarty, W.; Suárez, M.J.; Todling, R.; Molod, A.; Takacs, L.; Randles, C. A.; Darmenov, 1173 A.; Bosilovich, M. G.; Reichle, R.; Wargan, K.; Coy, L.; Cullather, R.; Draper, C.; Akella, S.; 1174 Buchard, V.; Conaty, A.; da Silva, A. M.; Gu, W.; Kim, G.; Koster, R.; Lucchesi, R.; Merkova, D.; 1175 Nielsen, J. E.; Partyka, G.; Pawson, S.; Putman, W.; Rienecker, M.; Schubert, S. D.; Sienkiewicz, M.; Zhao, B. The Modern-Era Retrospective Analysis for Research and Applications, Version 2 (MERRA-2). J. Climate, 30, 5419–5454
3. Randles, C. A.; da Silva, A. M.; Buchard, V.; Colarco, P. R.; Dar-menov, A.; Govindaraju, R.; Smirnov, A.; Holben, B.; Ferrare,R.; Hair, J.; Shinozuka, Y.; Flynn, C. The MERRA-2 aerosol reanalysis, 1980 onward. Part I: System description and data assimilation evaluation. J. Clim., 30(17), 6823-6850.
4. Hatzianastassiou, N.; Matsoukas, C.; Drakakis, E.; Stackhouse Jr., P.; Koepke, P.; Fotiadi,A.; Pavlakis, K.; Vardavas, I. The direct effect of aerosols on solar radiation based on satellite observations, reanalysis datasets, and spectral aerosol optical properties from Global Aerosol Data Set (GADS). Atmos. Chem. Phys. 7, 2585–2599.
5. Vardavas, I.; Carver, J.H. 1984. Solar and terrestrial parameterizations for radiative convective models. Planet. Space Sci. 32, 1307–1325.
6. Korras-Carraca, M.B.; Pappas, V; Hatzianastassiou, N.; Vardavas, I.; Matsoukas, C. Global vertically resolved aerosol direct radiation effect from three years of CALIOP data using the FORTH radiation transfer model Atmos. Res. 224, 138-156.
7. Hatzianastassiou, N.; Katsoulis, B.; Vardavas, I.. Sensitivity analysis of aerosol direct radiative forcing in ultraviolet–visible wavelengths and consequences for the heat budget. Tellus B 56, 368–381.
8. Wild, M., 2012. Enlightening Global Dimming and Brightening. Bull. Am. Meteorol. Soc. 93 (1),
9. Hatzianastassiou, N.; Matsoukas, C.; Fotiadi, A.; Stackhouse Jr., P.W.; Koepke, P.,Pavlakis, K.G.; Vardavas, I.. Modelling the direct effect of aerosols in the solar near-infrared on a planetary scale. Atmos. Chem. Phys. 7, 3211–3229.
10. Hansen, J., Sato, M.; Ruedy, R.: Radiative forcing and climate response, J. Geophys. Res., 102, 6831–6864, 1997.
11. Gkikas, A.; Obiso, V.; Pérez García-Pando, C.; Jorba, O.; Hatzianastassiou, N.; Vendrell, L.; Basart, S.; Solomos, S.; Gassó, S.; Baldasano, J. M. Direct radiative effects during intense Mediterranean desert dust outbreaks. Atmos. Chem. Phys. 18, 8757–8787.